HHS Public Access

Author manuscript

Biochem J. Author manuscript; available in PMC 2022 December 22.

Published in final edited form as:

Biochem J. 2021 December 22; 478(24): 4203–4220. doi:10.1042/BCJ20210644.

SLC26A9 is selected for endoplasmic reticulum associated degradation (ERAD) via Hsp70-dependent targeting of the soluble STAS domain

Patrick G. Needham[1], **Jennifer L. Goeckeler-Fried**[1], **Casey Zhang**[1,*], **Zhihao Sun**[1], **Adam R. Wetzel**[1,†], **Carol A. Bertrand**[2], **Jeffrey L. Brodsky**[1]

[1]Department of Biological Sciences, University of Pittsburgh, Pittsburgh, PA 15260, U.S.A

[2]Department of Pediatrics, University of Pittsburgh School of Medicine, Pittsburgh, PA 15261, U.S.A

Abstract

SLC26A9, a member of the solute carrier protein family, transports chloride ions across various epithelia. SLC26A9 also associates with other ion channels and transporters linked to human health, and in some cases these heterotypic interactions are essential to support the biogenesis of both proteins. Therefore, understanding how this complex membrane protein is initially folded might provide new therapeutic strategies to overcome deficits in the function of SLC26A9 partners, one of which is associated with Cystic Fibrosis. To this end, we developed a novel yeast expression system for SLC26A9. This facile system has been used extensively with other ion channels and transporters to screen for factors that oversee protein folding checkpoints. As commonly observed for other channels and transporters, we first noted that a substantial fraction of SLC26A9 is targeted for endoplasmic reticulum associated degradation (ERAD), which destroys folding-compromised proteins in the early secretory pathway. We next discovered that ERAD selection requires the Hsp70 chaperone, which can play a vital role in ERAD substrate selection. We then created SLC26A9 mutants and found that the transmembrane-rich domain of SLC26A9 was quite stable, whereas the soluble cytosolic STAS domain was responsible for Hsp70-dependent ERAD. To support data obtained in the yeast model, we were able to recapitulate Hsp70-facilitated ERAD of the STAS domain in human tissue culture cells. These results indicate that a critical barrier to nascent membrane protein folding can reside within a specific soluble domain, one that is monitored by components associated with the ERAD machinery.

Correspondence: Jeffrey L. Brodsky (jbrodsky@pitt.edu).
*Current address: University of Pittsburgh School of Medicine, Pittsburgh, PA 15261, U.S.A.
†Current address: Cleveland Clinic Foundation, Cleveland, OH 44103, U.S.A.

Competing Interests

The authors declare that there are no competing interests associated with the manuscript.

CRediT Author Contribution

Jeffrey L. Brodsky: Conceptualization, Resources, Formal analysis, Supervision, Funding acquisition, Validation, Writing — review and editing. **Patrick G. Needham:** Data curation, Formal analysis, Investigation, Visualization, Methodology, Writing — original draft. **Jennifer L. Goeckeler-Fried:** Formal analysis, Investigation, Visualization, Methodology, Writing — review and editing. **Casey Zhang:** Investigation, Visualization. **Zhihao Sun:** Investigation, Visualization. **Adam R. Wetzel:** Investigation, Visualization. **Carol A. Bertrand:** Conceptualization, Resources, Formal analysis, Funding acquisition, Methodology, Writing — review and editing.

Introduction

The regulation of salt and fluid balance across membranes is an essential function of epithelial cells, and to this end numerous ion channels and transporters are required to maintain cellular homeostasis. Consequently, mutations that interfere with the folding, transport, or activity of these channels and transporters to the cell surface can disrupt electrolyte balance and lead to disease [1-3]. For example, the Cystic Fibrosis Transmembrane Conductance Regulator (CFTR), is an epithelial chloride channel expressed most prominently in the lungs, the gastrointestinal tract, and sweat glands. To date, there are >2000 identified variants and ~300 disease-associated mutations which impact protein expression, channel activity, protein folding in the endoplasmic reticulum (ER), and the transport and stability of CFTR at the plasma membrane [4-6]. By far, the most common cause of CF arises from the F508del allele. The resulting mutant protein, which lacks a phenylalanine within the first nucleotide binding domain in CFTR, misfolds in the ER and fails to traffic beyond this organelle due to aggressive targeting to the ER associated degradation (ERAD) pathway [7-12]. While significant progress has led to the discovery of drugs that alleviate many CF symptoms [13,14], there remains a need for better and more widespread clinical treatments to correct defects associated with this allele as well as rare alleles [15,16]. Unfortunately, many of these disease-associated alleles are refractory to existing treatments.

CFTR directly influences chloride and water flux across epithelial membranes, but other ion transporting proteins similarly contribute to salt and fluid dynamics. Because these alternative chloride channels may function like CFTR, there is also a focus on identifying drugs that regulate the alternate transporters, thereby providing a means to rescue chloride secretion defects associated with mutant forms of CFTR, especially those that are refractory to current treatments [17,18]. Interestingly, some of these channels and transporters interact with CFTR.

One notable group of ion channels that associate with and co-regulate CFTR is the SLC26A proteins. The SLC26A family consists of 11 members that transport an array of mono- and divalent anions, such as Cl^-, OH^-, $NO3^-$, $HCO3^-$, and $SO4^-$ [19-21]. SLC26A proteins have a modular structure with a region enriched for membrane spanning helices followed by a large intracellular regulatory region, known as the STAS (sulfate transporter and anti-sigma factor antagonist) domain [20,22,23]. Early models suggested that SLC26A members contain 12 transmembrane helices (see Supplementary Figure S1 for a schematic of this topology for one SLC26A family member). More recent evidence suggests the presence of 14 transmembrane spanning segments [24-26]. Other data indicate that the ~34 kDa STAS domain mediates the dimerization of SLC26A proteins, and serves as a point of interaction with other proteins [26]. The extreme C-terminus of some family members also contains a small region — a PDZ motif — which in these cases can bridge SLC26A with protein partners, facilitates interactions with the STAS domain, and regulates the trafficking and degradation of SLC26 [20,27-29]. Interestingly, two members of the SLC26A family with chloride-bicarbonate exchange activity, SLC26A3 and SLC26A6, bind

the phosphorylated R-domain in CFTR through the STAS domain, which in turn increases both CFTR-dependent chloride flux as well as SLC26A anion exchange activity [30].

Yet another SLC26A family member, SLC26A9, is also emerging as an important CFTR regulator and potential drug target [30-38]. SLC26A9 acts as a constitutive chloride transporter; early studies suggested it could also exhibit anion exchange activity, like SLC26A3 and SLC26A6 [32,39-43], but recent structural analyses have failed to identify anion exchange behavior [26,44]. Moreover, polymorphisms in SLC26A9 are linked to several CF-associated phenotypes [45-48], and the response to drugs that potentiate the gating of a disease-causing allele in CFTR (G551D) is modulated by non-coding polymorphisms in SLC26A9 [49,50]. In addition, when SLC26A9 activity is enhanced in lung epithelia, this helps alleviate mucus build-up in response to inflammation [51], which is frequently seen in CF patients [52,53]. A significant body of work also indicates that both SLC26A9 and CFTR contribute to basal and stimulated chloride currents in human bronchial epithelia (HBE), but SLC26A9 currents are absent from CF patient tissue [4,30,31,39,54-57]. Yet, other data indicate SLC26A9 exhibits chloride transport activity even in the absence of CFTR expression [33,40,43]. Indeed, when SLC26A9 is co-expressed with F508del CFTR in model cell types, SLC26A9 currents are absent [32]. Moreover, when the biogenesis and activity of F508del CFTR are partially rescued by low temperature or by a protein folding corrector compound, cell surface expression of SLC26A9 also increases and SLC26A9 currents are again detected [35]. Although SLC26A9 is also turned over by the ERAD pathway when co-expressed with F508del CFTR, transfection of wild-type CFTR into F508del CFTR-expressing cells increases SLC26A9 trafficking to the plasma membrane [38]. Together, these results reveal that F508del CFTR prevents SLC26A9 trafficking to the plasma membrane and increases the degradation of ER-retained SLC26A9.

Although a significant body of work indicates that SLC26A9 might be modulated to overcome symptoms associated with CF, cellular chaperones that facilitate SLC26A9 maturation or degradation in the early secretory pathway are unknown. This undertaking is vital as drugs that target many of these chaperones are being developed [58-60]. To identify factors that contribute to the biogenesis of other ion channels and transporters, we have made extensive use of yeast expression systems. In all cases, the identified chaperones functioned similarly in higher cells [61-68]. We now report that a significant portion of SLC26A9 is targeted for ERAD in yeast, as in mammalian cells, and discovered that substrate ubiquitination and degradation are mediated by the cytoplasmic Hsp70 molecular chaperone. A dissection of the SLC26A9 protein next revealed that the STAS domain is highly unstable, and like the full-length protein, its turnover required Hsp70 activity. Protein stability measurements in HEK293 cells support an analogous requirement for Hsp70 during STAS domain degradation in mammals. Overall, this study defines a specific folding barrier during SLC26A9 maturation and provides a platform to dissect the contributions of SLC26A9 polymorphisms on protein stability and selection for chaperone-dependent ERAD.

Materials and methods

Yeast strains, plasmid construction, and protein expression

All yeast strains used in this study are listed in Supplementary Table S1. Plasmids containing the coding sequences of the two full length forms of SLC26A9 and the free STAS domain were obtained in a pcDNA3.1 vector [32,35]. Yeast expression vectors were constructed by PCR amplification of the SLC26A9 coding sequence, incorporating restriction sites for SpeI and Cla1 at the 5′ and 3′ ends of the gene, respectively, and with the addition of a c-myc tag (EQKLISEEDL) at the N-terminus of the protein. The amplified DNA was digested with the SpeI and Cla1 enzymes, gel purified, and ligated into the multicopy histidine-selectable yeast expression vector pRS423MET [69], which had been digested with the same enzymes. This created plasmids 423MET-A9-1 and 423MET-A9-2, in which SLC26A9 expression is controlled by the methionine-repressible *MET25* promoter. A yeast expression vector for the STAS domain was similarly created by PCR amplifying an N-terminal c-myc tagged coding sequence starting at amino acid 505 of SLC26A9 isoform 1 and incorporating Spe1 and Cla1 restriction sites into the primers for ligation into pRS423MET. In turn, the SLC26A9 construct truncated after the transmembrane region (Δstas) was created by introducing a stop codon into the sequence of full length SLC26A9 isoform 1 at lysine 518 using the Quick Change II Site Directed Mutagenesis Kit (Agilent) and primer sequences 5′-gacatttatgtgaatccctagacctataatagggccc-3′ and 5′-gggccctattataggtctagggattcacataaatgtc-3′. All candidate plasmids were screened by restriction digest and verified by DNA sequencing (GeneWiz). To utilize methionine auxotrophic yeast strains, such as BY4741 and *hrd1Δ asi1*Δ with our SLC26A9 *MET25* promoter expression system, we restored the *MET15* locus in these strains to allow for growth in -Met media. To this end, the *MET15* locus [70] was first PCR amplified from BY4742 genomic DNA using primers 5′-tagctctcattatttttgctttttctcttgaggtcaca-3′ and 5′-ttgttgaatgttgagcaagttaacatcttataggacatat-3′. The amplified DNA was introduced into the yeast genome by homologous recombination and the cells were selected on SC media lacking methionine (SC-Met). Colonies were re-streaked onto SC-Met plates two additional times to ensure *MET15* integration.

To express each protein, the indicated vectors were introduced into yeast using lithium acetate transformation [71] and selected on synthetic complete media lacking histidine but supplemented with methionine at a final concentration of 0.5 mM (SC-His + Met). Yeast transformed with the indicated expression plasmid(s) were then grown in liquid media overnight from single colonies in the appropriate selective media at room temperature. The cells were washed in sterile water, resuspended at an optical density (OD_{600}) of 0.5 in SC-His-Met to induce protein expression from the Met-repressible promotor, and growth was continued for 2–3 h at 30°C with shaking. These cultures were then transferred to a shaking water bath at 30°C or shifted for the indicated times to 37°C for assays in temperature sensitive mutant strains.

Measurements of protein stability, ubiquitination, and membrane association in yeast

Protein translation was arrested by addition of cycloheximide to a final concentration of 100 μg/ml, and equal aliquots of cells were removed at the indicated times. The assay

was performed at 30°C unless otherwise indicated (i.e. for the temperature sensitive yeast strains). In this case, cells were maintained at the elevated temperature throughout the chase. In all cases, cells were collected by centrifugation at 13 000 RPM in a Sorvall microcentrifuge for 1 min at 4°C, quick frozen in liquid nitrogen, and the cell pellets were stored at −80°C. To prepare protein fractions, the cell pellets were thawed, and total protein was extracted by trichloroacetic acid (TCA) precipitation [72]. Protein samples were suspended in sample buffer and resolved by SDS–PAGE.

Following SDS–PAGE, proteins were transferred to nitrocellulose membranes and a quantitative Western Blot analysis was performed. The quality of the load and transfer was assessed by Ponceau-S staining of the membrane for every blot before antibody incubation. SLC26A9 was detected with rabbit polyclonal anti-myc (Santa Cruz A-14) and anti-rabbit HRP-conjugated secondary antibody (CST). Rabbit anti–glucose-6-phosphate dehydrogenase (G6PD) (A9521; Sigma–Aldrich) was used as a loading control. The blots were then incubated with the ECL reagent (Prometheus ProSignal), visualized on a Bio-Rad imager, and quantified with Image-J software. All statistical analyses were performed using GraphPad Prism 8 (GraphPad Software, Inc., CA, US). The amount of protein at time 0 was set to 100%, and the remaining time points were expressed as a percent of the starting material. Only data with a $P < 0.05$ was considered significant.

To measure protein ubiquitination [73], cells engineered for STAS domain expression were transformed with pLHP462, an HA-tagged ubiquitin expression plasmid under the control of the copper inducible *CUP1* promoter [74]. The expression of the c-myc tagged STAS domain was induced as described above, and after 1 h, Ub-HA expression was induced by the addition of CuSO4 to a final concentration of 100 μM. A 40 ml culture of the *pdr5Δ* yeast strain was then split and treated with MG-132 at a final concentration of 100 μM or with an equal volume of DMSO at 30°C in a shaking water bath for 1 h. *SSA1* or *ssa1–45* yeast were instead shifted to 37°C in a shaking water bath for 30 min before cells were treated with 10 mM (final concentration) NaN_3 and quickly cooled in an ice/water bath. In all cases, cells were centrifuged in a tabletop clinical centrifuge at 4000 RPM, and the resulting cell pellets were stored at −80°C. Next, the pellets were thawed and resuspended in 50 mM Tris, pH 7.4, 150 mM NaCl, 5 mM EDTA, 1% Triton-X100, 1% SDS, 10 mM *N*-ethylmaleimide, 1 mM PMSF, 1 μg/ml leupeptin, and 0.5 μg/ml pepstatin A, and the cells were disrupted by agitation with glass beads and debris was removed by centrifugation at 10 000g for 1 min. Clarified lysate was diluted with resuspension buffer lacking SDS to a final concentration of 0.2% SDS. Anti-myc conjugated to agarose (Pierce) pre-equilibrated in the same buffer was then added to the clarified lysate, and the mixture was rotated overnight at 4°C. The beads were subsequently collected by centrifugation at 500***g***, the supernatant was removed by pipetting, and the beads were washed three times in the same buffer. The bound protein was removed from the beads by incubation in SDS–PAGE sample buffer at 42°C for 30 min. Following SDS–PAGE, an immunoblot analysis was performed using anti-c-myc antibody to detect the STAS domain (see above) or HRP-conjugated anti-HA antibody (Roche) to detect ubiquitinated protein.

To determine the degree to which a specific protein associated with organellar membranes, cells expressing each SLC26A9 construct were harvested by centrifugation. Cell lysate was

prepared by resuspending cells in lysis buffer (0.1 M sorbitol, 50 mM potassium acetate (KOAc), 2 mM EDTA, 20 mM HEPES-NaOH, pH7.4) in the presence of 1 mM PMSF, 1 μg/ml leupeptin, and 0.5 μg/ml pepstatin A, and the cells were disruption by agitation with glass beads. Debris was removed by centrifugation for 2 min at 2000 RPM in a tabletop clinical centrifuge. The resulting supernatant was transferred to a clean tube and the membranes pelleted by centrifugation at 20 000***g*** for 15 min. The pellet fraction (P1) was resuspended in lysis buffer, split into separate tubes and pelleted again at 20 000***g*** for 15 min. Association was detected using specific treatments as described [75]. Briefly, the P1 fraction was suspended in either lysis buffer or lysis buffer containing 6 M urea and the tubes were rotated at 4°C for 1 h. After treatment, the solutions were centrifuged at 25 000g and the supernatant (S2) was removed from the pellet (P2). Each of these fractions was analyzed by SDS–PAGE and western blotting. Controls included Pma1 (an integral membrane protein), Pdi1(a peripheral membrane-associated protein in the ER), and G6PD (a soluble protein).

Mammalian cell protein stability assays

HEK293 cell cultures were maintained in DMEM (Sigma–Aldrich) supplemented with 10% FBS (Seradigm premium grade) at 37°C in a 5% CO_2 humidified atmosphere. At 24 h prior to transfection, 0.6×10^6 cells were plated into wells of a six-well poly-L-lysine coated plate (Greiner BioOne) with 3 ml DMEM containing 10% FBS per well. Transfections with pcDNA3.1 engineered for the expression of the STAS domain [76] included 2 μg of plasmid DNA and 6 μl of Lipofectamine™ 2000 (Thermo Fisher Scientific #11668) per well, suspended in a total volume of 500 μl Opti-MEM (Thermo Fisher Scientific #31985) per well, according to the manufacturer's protocol. The media was then changed after 6 h. Experiments were conducted 24 h after transfection.

To perform cycloheximide chase assays, the cells were pre-treated with 10 μM MG-132 (EMD Millipore) for 2 h, the media was removed and replaced with DMEM containing 10% FBS as well as 20 μg/ml cycloheximide (Sigma), and then either 10 μM MG-132, 25 μM VER155008 (Tocris), or an equivalent volume of DMSO was added. At the indicated times, the media was aspirated from the wells, and the cells were lysed in 300 μl of ice-cold TNT Buffer (50 mM Tris, pH 7.2, 150 mM NaCl, 1% Triton X-100) with a complete protease inhibitor cocktail (Roche). During this time, plates were incubated on ice for 30 min with gentle rocking, and the solution was removed and centrifuged at ~16 000***g*** for 10 min at 4°C. The cleared lysate was diluted into SDS Sample Buffer. Total protein was resolved on 10% polyacrylamide gels by SDS–PAGE and transferred to nitrocellulose. To assess protein loading, blots were stained with the REVERT total protein staining kit (Licor) and imaged in the 700 channel of a Licor Odyssey CLX. The stain was then reversed, the blots were blocked in TBST-milk solution for 1 h, and the myc-tagged STAS protein was detected with clone 9E10 (Biolegend) at a 1 : 250 dilution. Bound antibodies were decorated for 2 h with goat anti-mouse IRdye800 antibody (Licor), diluted 1 : 15 000, and imaged in the 800 channel of a Licor Odyssey CLX.

For experiments in which the steady-state levels of the STAS domain were examined in HEK293 cells, the cells were transfected as above and then treated with VER155008 or an

equivalent volume of DMSO at the final concentrations indicated above. The cells were then incubated for 2 h and processed for immunoblotting, as above, except that a 1 : 500 antibody dilution of the anti-myc antibody was used.

Results

To determine whether SLC26A9 is prone to misfolding in the ER — as observed for other polytopic membrane ion channels [77] — and to identify the factors that control its stability and degradation, we developed a yeast SLC26A9 expression system. The yeast model has been used extensively to identify chaperones and chaperone-like proteins that regulate the stability of human ion channels and transporters, and in nearly all cases the results uncovered from this organism have been recapitulated in human cells [61-68].

To this end, we first constructed a regulated expression system for two SLC26A9 isoforms in yeast. The isoforms differ by 96 amino acids [36] (Supplementary Figure S1), and to date their relative stabilities in the ER have not been investigated. The expression of these proteins was under the control of the methionine repressible *MET25* promoter, which allowed for SLC26A9 expression to be repressed on media containing methionine and then quickly activated by resuspending cells in methionine-free media. Next, each plasmid was introduced into wild-type yeast, and a time course after incubation in methionine-free media indicated rapid expression of both isoforms after 1 h with peak levels reached by 4 h (Supplementary Figure S2A). To measure the stability of the SLC26A9 isoforms in yeast, we then conducted a cycloheximide chase assay after protein expression had been derepressed for 2 h. As shown in Supplementary Figure S2B, SLC26A9 — like wild-type and F508del CFTR in yeast [61-63] — was unstable and degraded over time. Furthermore, the degradation rates of isoforms 1 and 2 were indistinguishable in this strain or in other strains examined (Supplementary Figure S2B and data not shown). Therefore, we conducted all experiments in this study using the more commonly described isoform 1 [78].

Since SLC26A9 was rapidly degraded after a translation shut-off, we investigated if degradation was via ERAD or an alternative post-ER degradation pathway [79]. ERAD substrates are targeted for degradation via the ubiquitin-proteasome pathway [80-82], so we first asked whether SLC26A9 degradation was proteasome-dependent. To allow robust proteasome inhibition with MG-132, we utilized a *PDR5*-deficient yeast strain as it lacks a drug efflux pump [83]. As shown in Figure 1A, MG-132 treatment resulted in significant SLC26A9 stabilization over the time course of the assay. We next performed cycloheximide chase assays in a yeast strain deficient in the two major ER-associated E3 ubiquitin ligases, Hrd1 and Doa10 [84,85] (Figure 1B). The absence of the genes encoding *HRD1* and *DOA10* also resulted in significant SLC26A9 stabilization, strongly suggesting that the ERAD pathway eliminates SLC26A9. Interestingly, deletion of either E3 ligase only subtly stabilized the protein (data not shown), suggesting that both enzymes work together to most efficiently target this complex substrate for degradation.

Ubiquitinated ERAD substrates must be extracted or ‘retrotranslocated’ from the ER prior to or concomitant with proteasome-dependent degradation [86,87]. Therefore, we examined whether Cdc48, which drives the ATP-dependent retrotranslocation of ERAD

substrates, was also required for SLC26A9 degradation. As anticipated, inactivation of a thermosensitive *CDC48* allele led to profound stabilization of SLC26A9 in a cycloheximide chase assay (Figure 1C). Although these data further support the role of ERAD in SLC26A9 turnover, we also excluded another major location of protein degradation in yeast, the vacuole (which is the yeast lysosome equivalent). Yeast lacking Pep4, which express <5% of residual vacuolar protease activity [88], still efficiently degraded SLC26A9 (Figure 1D). This is in stark contrast with the dramatic stabilization of a known vacuolar substrate SZ* in *pep4Δ* yeast ([89] and see for example Supplementary Figure S4B). Taken together, we conclude that ER quality control accounts for the degradation of immature, ER-resident SLC26A9 species in yeast, as suggested by studies performed previously in higher cells [38].

Cytoplasmic Hsp70 molecular chaperones bind misfolded proteins and can contribute to the recognition of misfolded substrates in the ER, which are then delivered to ubiquitin ligases such as Doa10 [90,91]. For substrates that deposit misfolded domains in the ER lumen, a lumenal Hsp70 (BiP) similarly recognizes misfolded proteins in this compartment and prevents substrate aggregation, which favors retrotranslocation [92,93]. To determine if the cytoplasmic and/or lumenal Hsp70 chaperones facilitate SLC26A9 degradation, cycloheximide chases were performed in yeast expressing a temperature-sensitive mutant form of the major cytoplasmic Hsp70 that lacks the other primary cytoplasmic Hsp70s (*ssa1–45*, *ssa2*, *ssa3*, *ssa4*) [94], or that contain an ERAD-specific BiP (*kar2-1*) mutant [95]. Upon a shift to 37°C, SLC26A9 was significantly stabilized in the *ssa1–45* strain (Figure 2A). Importantly, the magnitude of stabilization was similar to that seen in the ERAD-deficient strains (Figure 1A-C). In contrast, the degradation of SLC26A9 in *kar2-1* yeast was unaffected compared with the wild-type strain, indicating that this ER lumenal Hsp70 most likely does not select SLC26A9 for degradation (Figure 2B). More generally, these data suggest that the misfolded domain that contributes to the selection of SLC26A9 for ERAD resides in the cytosol, i.e. the ~34 kDa STAS domain (Supplementary Figure S1).

To more definitively determine which region of the protein is recognized by the ERAD machinery, we constructed several versions of the protein. These included full length SLC26A9, a form of SLC26A9 that terminates at amino acid 517 which is before the start of the STAS domain at amino acid 520 (‘Δstas’), and a membrane domain-free version of the STAS domain beginning immediately after the transmembrane region at amino acid 505 (Supplementary Figure S1B). Each species also contained an N-terminal myc epitope tag for detection. We then performed cycloheximide chases to determine the relative stabilities of each protein.

We first noted that the transmembrane-only Δstas species was degraded much slower than full length SLC26A9 in wild-type yeast, although the modest level of measured degradation was reduced in a strain lacking Hrd1 and Doa10 E3 ligases (Figure 3A), as observed for the full-length protein (Figure 1B). Second, and as noted above, most ERAD substrates with misfolded cytosolic domains are degraded in an Hsp70-dependent manner (or in yeast, in an Ssa1-dependent manner) [90,91]. Therefore, we also examined whether disabling this chaperone through the use of the thermosensitive *ssa1–45* mutant slowed Δstas degradation. As anticipated based on the lack of a misfolded cytoplasmic region, Δstas turnover was

Ssa1-independent (Figure 3B), again suggesting that the STAS domain was responsible for Hsp70-dependent degradation. Third, and consistent with our hypothesis, we discovered that the turnover of the isolated STAS domain was almost completely blocked when the yeast Hsp70, Ssa1, was disabled (Figure 4A). Therefore, Hsp70 appears to recognize and target full-length SLC26A9 by virtue of the cytosolic STAS domain. Finally, as a control, we established that the STAS domain was also strongly stabilized by treating cells with MG-132 (Figure 4B).

In contrast to full-length SLC26A9 (Figure 1B), the STAS domain was degraded at the same rate when Hrd1 and Doa10 were lacking (Figure 5A). These results implied that STAS proteolysis required an alternate E3 ubiquitin ligase, an outcome that is frequently observed when the degradation of misfolded cytoplasmic proteins is examined [75,96,97]. Therefore, we first examined STAS domain stability when two cytoplasmic quality control E3s, San1 and Ubr1 [96,97], were absent, but again the protein was degraded proficiently (Figure 5B). As a control, we confirmed that an established ERAD substrate, CPY*, as well as a cytoplasmic misfolded protein, NBD2* [75,98], were stabilized in *hrd1Δ doa10*Δ and *san1Δ ubr1*Δ yeast, respectively (Supplementary Figure S3A,B). STAS domain degradation was also unaffected in *pep4Δ* yeast (Supplementary Figure S4A).

Some misfolded proteins enter the nucleus and their degradation is facilitated by the Asi1-containing ubiquitin ligase complex, which resides in the inner nuclear membrane, and Hrd1 can aid in the turnover of these substrates [99,100]. Therefore, we assessed STAS domain stability in a *hrd1Δ asi1*Δ strain. As a control, we first established that a model ERAD substrate, CPY*, was stabilized in this mutant (Supplementary Figure S3C). While the overall degradation of STAS was rapid, there was a small but statistically significant stabilization of STAS when both *HRD1* and *ASI1* were deleted (Figure 5C). Finally, we examined STAS domain turnover in strains containing a thermosensitive version of *RSP5*, which encodes a cytosolic ubiquitin ligase that plays critical roles in plasma membrane protein endocytosis [101,102]. However, Rsp5 has also been reported to contribute to other quality control phenomena [103-105]. When STAS degradation was analyzed in the temperature sensitive *rsp5-1* mutant after a shift to the non-permissive 38°C, we again saw modest but statistically significant stabilization (Figure 5D). Interestingly, Rsp5 was reported to contribute to the degradation of heat-damaged proteins in yeast [106], suggesting that STAS might assume a non-native structure mimicking that attained by a thermolabile protein. Based on these collective results, it is likely that a compendium of E3 ubiquitin ligases, which includes Hrd1, Asi, and Rsp5, contributes promiscuously to the quality control of STAS, an outcome that is not uncommonly seen [107]. Future efforts will seek to better define the ligase ensemble that mediates STAS degradation.

To confirm that STAS domain degradation was ubiquitin-dependent, we immunoprecipitated the domain from cell lysates prepared from *pdr5Δ* yeast treated with either DMSO or MG-132 (to demonstrate ubiquitinated protein targeting to the proteasome), and from wild-type (*SSA1*) and *ssa1–45* yeast after a shift to the non-permissive temperature (Figure 6). Analysis of STAS ubiquitination was facilitated by co-expression with HA epitope-tagged ubiquitin, which can be readily detected and quantified. As shown in Figure 6A, the STAS domain was ubiquitinated, and as expected for a proteasome-targeted substrate, the relative

amount of ubiquitination increased upon MG-132 treatment. Because STAS degradation also required Hsp70 (Ssa1) function (Figure 4A), we then asked if Ssa1 activity was required for STAS ubiquitination. Therefore, STAS ubiquitination was measured at 26°C and 38°C both in the wild-type and in the *ssa1–45* mutant strain. Although total protein ubiquitination increased in both strains after a shift to the higher temperature (Figure 6B, top panel, input lanes) relative to the amount of STAS in the load (see 'Myc-STAS'), there was a modest reduction in the amount of STAS ubiquitination when the precipitated protein was examined in lysates prepared from the *ssa1–45* mutant (Figure 6B, bottom). These results are consistent with Hsp70 aiding in the delivery of the STAS domain to the ubiquitination machinery. However, because STAS domain ubiquitination was not entirely blocked in the mutant, it is possible that Ssa1 also contributes to the delivery of ubiquitinated STAS adducts to the proteasome (but see Discussion).

Since Hsp70 supports the targeting of substrates to both the ERAD and cytoplasmic quality control pathways [72,87], we asked whether the STAS domain is completely cytosolic, is membrane-associated, or is unexpectedly integrated into the membrane. When total lysate was subjected to high-speed centrifugation analysis to pellet the membranes (Figure 7A), full length SLC26A9 and the Δstas protein were found associated with the initial pellet (P1) fraction, as was the integral membrane protein Pma1 (Figure 7B,C). Further treatment of P1 with buffer or with 6 M urea failed to remove significant amounts of these proteins from the final membrane fraction (P2), in-line with their expected membrane integration. In contrast, and as expected, the peripheral membrane-associated Pdi1 protein was partially liberated from the P2 membranes with urea. Also as expected, the soluble G6PD protein was found in the S1 fraction.

We then examined the behavior of the STAS domain. We found that this domain was membrane associated after the initial fractionation (Figure 7D, P1 fraction), but consistent with a lack of membrane integration the STAS domain was removed from the membranes with urea (Figure 7D, lane S2 'Urea'). Thus, STAS appears to be membrane-associated in yeast, perhaps consistent with its targeting by multiple ubiquitin ligases (see above), i.e. those that are both membrane-associated and that reside in the cytosol.

Prior work confirmed that chaperone requirements for the degradation of misfolded proteins in yeast can be translated into mammalian cells (see Introduction), even though in some cases the relative magnitude of post-ER quality control (i.e. lysosome-dependent degradation) versus ERAD is higher in human cells relative to yeast (see for example [66]). Therefore, we expressed the STAS domain in HEK293 cells. We first confirmed that STAS domain degradation was proteasome- (i.e. MG-132) dependent: As observed in yeast, the domain was degraded over time but was stabilized by treatment with MG-132 (Figure 8A,B). Next, to determine if Hsp70 facilitates STAS domain degradation in mammalian cells as it does in yeast, cycloheximide chases were again performed, but since thermosensitive Hsp70 mutant alleles are unavailable in higher cells, the cells were instead incubated with an Hsp70 inhibitor, VER155008, which blocks the ATP-binding site in Hsp70 but has no effect on the activity of other ATP-requiring chaperones, such as Hsp90 [108]. Although there was a lag-time for the effect of the compound to become apparent, STAS domain turnover was also slowed after 3 h when Hsp70 activity was inhibited with VER155008. To confirm these

results, we modified the assay to examine the steady-state levels of STAS in the HEK293 cells after treatment with VER155008 (Figure 8C). Based on this analysis, STAS levels in the cell were ~2-fold higher in the presence of VER155008 compared with the DMSO control. Our combined results establish that Hsp70 is required for the degradation of the soluble STAS domain in both yeast and human cells. Our results additionally suggest that the recognition of full-length SLC26A9 for ERAD is initiated by the selective capture of the STAS domain by Hsp70.

Discussion

We report on the first analysis of the molecular requirements that lead to the selection and targeting of SLC26A9, a CFTR-interacting ion channel, for ERAD. To this end, we developed a new SLC26A9 inducible expression system in the yeast *S. cerevisiae*, an organism that allows for the rapid genetic dissection of the myriad pathways that lead to the disposal of immature ion channels and transporters by the ERAD pathway [109]. Interestingly, a non-trivial fraction of even the wild-type forms of many ion channels and transporters appear to fold inefficiently, an outcome that leads to ERAD targeting. For example, well over half of CFTR is selected for ERAD when stability is assessed in model cell types [7], although the level might be somewhat different when cells are propagated under more native-like conditions [110]. Our data indicate that SLC26A9 — and most notably the STAS domain — is no different: in both yeast and HEK293 cells, the STAS domain is also relatively unstable. These results are consistent with previous reports demonstrating that large quantities of insoluble SLC26A9 accumulate in BHK cells after treatment with MG-132 [38]. In the future, it will be important to measure whether SLC26A9 or CFTR mutants enhance the targeting of SLC26A9 for ERAD, a phenomenon that is commonly noted when CFTR or other ion channels and transporters harbor disease-associated alleles [77].

For many ERAD substrates, the domain or domains that target a protein for the ERAD pathway are poorly defined. In yeast, model ERAD substrates can be binned into ERAD-C, ERAD-M, and ERAD-L substrates, depending on whether the major folding lesion resides in the cytosol, membrane, or ER lumen, respectively [111]. In reality, however, defects in a single domain might impact the integrity of other regions within the protein, and indeed the categorization of ERAD substrates into these three distinct groups breaks down when select proteins are examined in yeast [112] or higher cells [113]. In contrast, the selection of SLC26A9 appears to represent a relatively ‘clean’ example of an ERAD-C substrate since the overall stability of the protein is dictated to a large extent by a single cytosolically disposed domain, i.e. the STAS domain. In addition, the Hsp70-dependence on the degradation of this domain almost fully accounts for the Hsp70-dependent degradation of the full-length protein. We also show that Hsp70 helps target SLC26A9 to the ubiquitin pathway, since disabling Hsp70 (via the use of the thermosensitive Ssa1 mutant) reduced substrate ubiquitination, although not completely. This might arise from the *ssa1–45* allele retaining partial function under the conditions of the experiment, or due to the fact that Hsp70 also acts after substrate ubiquitination. Because inhibiting CFTR ubiquitination augments the correction of the F508del CFTR mutant by FDA-approved drugs [114,115],

it is possible that similar strategies might one day be used to improve the biogenesis of trafficking-defective SLC26A9 mutants.

One surprising aspect of this study is that — given the complexity of the transmembrane domain of SLC26A9, which possesses 14 individual membrane-spanning helices — the folding efficiency of this domain is high, i.e. the Δstas construct was quite stable. This contrasts with the noted instability of transmembrane domain-containing proteins that are at least partially selected for ERAD-M in yeast [112,116,117]. In fact, a recent cryo-EM structure of SLC26A9 indicates that the transmembrane region is built to allow for uncoupled chloride transport [26]. However, unlike most oligomeric ion channels that possess multiple transmembrane segments, the formation of the SLC26A9 dimer is not mediated by the transmembrane domains. Instead, the transmembrane domains may fold independently of SLC26A9 dimerization, which could explain the relative stability of the Δstas construct.

In contrast to the transmembrane region, we suggest that the STAS domain folds inefficiently, i.e. it is unstable in both yeast and human cells. The STAS domain — and especially the N-terminal portion of the domain — is responsible for the interaction between the two SLC26A9 molecules in the dimer [26]. Thus, it is possible that the post-translational association between two STAS domains as SLC26A9 dimerizes in the cell represents a rate-limiting and problematic step in the folding pathway. Moreover, the STAS domain possesses an intrinsically disordered region that might lead to further destabilization. The PDZ tail also contains a putative disordered region. Intriguingly, the removal of these regions improves SLC26A9 cell surface residence and solubility in detergent [26]. Future work will be undertaken to test these and other hypotheses on the rate-limiting steps in the SLC26A9 folding pathway.

In conclusion, our work shows that complex, polytopic membrane proteins can possess both relatively stable as well as unstable domains whose contributions on overall stability can be differentiated. Moreover, the unstable domain can, in effect, function as a ‘degron’ [118]. In other words, a motif (such as STAS) when attached to a stable polypeptide (i.e. Δstas) is sufficient to direct the fusion protein to the ubiquitin-proteasome system. By dissecting the contributions of each domain, we also discovered that — consistent with prior studies — the Hsp70 chaperone facilitates the delivery of SLC26A9 to the ubiquitination machinery. Based on the importance of SLC26A9 in health and disease, and the generation of drugs that modify protein folding and chaperone function [58,119], our study serves as a first step toward the goal of regulating SLC26A9 stability alone or in combination with vital partners, such as CFTR.

Supplementary Material

Refer to Web version on PubMed Central for supplementary material.

Funding

This work was supported by NIH grants P30 DK079307 and R35 GM131732 to J.L.B., and by grants BERTRA12G0 and BERTRA17P0 from the Cystic Fibrosis Foundation to C.A.B. We thank Dr. Ally O'Donnell, for valuable discussions and reagents.

Data Availability

All original data related to work described in this paper are available from the authors upon request.

Abbreviations

CFTR	Cystic Fibrosis Transmembrane Conductance Regulator
ER	endoplasmic reticulum
ERAD	endoplasmic reticulum associated degradation
G6PD	anti–glucose-6-phosphate dehydrogenase
STAS	sulfate transporter and anti-sigma factor antagonist

References

1. O'Donnell BM, Mackie TD and Brodsky JL (2017) Linking chanelopathies with endoplasmic reticulum associated degradation. Channels (Austin) 11, 499–501 10.1080/19336950.2017.1357944 [PubMed: 28723237]
2. Salih M, Gautschi I, van Bemmelen MX, Di Benedetto M, Brooks AS, Lugtenberg D et al. (2017) A missense mutation in the extracellular domain of alphaENaC causes liddle syndrome. J. Am. Soc. Nephrol 28, 3291–3299 10.1681/ASN.2016111163 [PubMed: 28710092]
3. Kokunai Y, Nakata T, Furuta M, Sakata S, Kimura H, Aiba T et al. (2014) A Kir3.4 mutation causes Andersen-Tawil syndrome by an inhibitory effect on Kir2.1. Neurology 82, 1058–1064 10.1212/WNL.0000000000000239 [PubMed: 24574546]
4. Welsh MJ and Smith AE (1993) Molecular mechanisms of CFTR chloride channel dysfunction in cystic fibrosis. Cell 73, 1251–1254 10.1016/0092-8674(93)90353-R [PubMed: 7686820]
5. Mall MA and Hartl D (2014) CFTR: cystic fibrosis and beyond. Eur. Respir. J 44, 1042–1054 10.1183/09031936.00228013 [PubMed: 24925916]
6. Veit G, Avramescu RG, Chiang AN, Houck SA, Cai Z, Peters KW et al. (2016) From CFTR biology toward combinatorial pharmacotherapy: expanded classification of cystic fibrosis mutations. Mol. Biol. Cell 27, 424–433 10.1091/mbc.e14-04-0935 [PubMed: 26823392]
7. Cheng SH, Gregory RJ, Marshall J, Paul S, Souza DW, White GA et al. (1990) Defective intracellular transport and processing of CFTR is the molecular basis of most cystic fibrosis. Cell 63, 827–834 10.1016/0092-8674(90)90148-8 [PubMed: 1699669]
8. Lukacs GL, Chang XB, Bear C, Kartner N, Mohamed A, Riordan JR et al. (1993) The delta F508 mutation decreases the stability of cystic fibrosis transmembrane conductance regulator in the plasma membrane. determination of functional half-lives on transfected cells. J. Biol. Chem 268, 21592–8 10.1016/S0021-9258(20)80582-1 [PubMed: 7691813]
9. Lukacs GL, Mohamed A, Kartner N, Chang XB, Riordan JR and Grinstein S (1994) Conformational maturation of CFTR but not its mutant counterpart (delta F508) occurs in the endoplasmic reticulum and requires ATP. EMBO J. 13, 6076–6086 10.1002/j.1460-2075.1994.tb06954.x [PubMed: 7529176]

10. Jensen TJ, Loo MA, Pind S, Williams DB, Goldberg AL and Riordan JR (1995) Multiple proteolytic systems, including the proteasome, contribute to CFTR processing. Cell 83, 129–135 10.1016/0092-8674(95)90241-4 [PubMed: 7553864]
11. Ward CL, Omura S and Kopito RR (1995) Degradation of CFTR by the ubiquitin-proteasome pathway. Cell 83, 121–127 10.1016/0092-8674(95)90240-6 [PubMed: 7553863]
12. Xiong X, Chong E and Skach WR (1999) Evidence that endoplasmic reticulum (ER)-associated degradation of cystic fibrosis transmembrane conductance regulator is linked to retrograde translocation from the ER membrane. J. Biol. Chem 274, 2616–2624 10.1074/jbc.274.5.2616 [PubMed: 9915789]
13. Collins FS (2019) Realizing the dream of molecularly targeted therapies for cystic fibrosis. N. Engl. J. Med 381, 1863–1865 10.1056/NEJMe1911602 [PubMed: 31670919]
14. Heijerman HGM, McKone EF, Downey DG, Van Braeckel E, Rowe SM, Tullis E et al. (2019) Efficacy and safety of the elexacaftor plus tezacaftor plus ivacaftor combination regimen in people with cystic fibrosis homozygous for the F508del mutation: a double-blind, randomised, phase 3 trial. Lancet 394, 1940–1948 10.1016/S0140-6736(19)32597-8 [PubMed: 31679946]
15. Sosnay PR, Siklosi KR, Van Goor F, Kaniecki K, Yu H, Sharma N et al. (2013) Defining the disease liability of variants in the cystic fibrosis transmembrane conductance regulator gene. Nat. Genet 45, 1160–1167 10.1038/ng.2745 [PubMed: 23974870]
16. Li H, Pesce E, Sheppard DN, Singh AK and Pedemonte N (2018) Therapeutic approaches to CFTR dysfunction: from discovery to drug development. J. Cyst. Fbros 17, S14–S21 10.1016/j.jcf.2017.08.013
17. Li H, Salomon JJ, Sheppard DN, Mall MA and Galietta LJ (2017) Bypassing CFTR dysfunction in cystic fibrosis with alternative pathways for anion transport. Curr. Opin. Pharmacol 34, 91–97 10.1016/j.coph.2017.10.002 [PubMed: 29065356]
18. Quesada R and Dutzler R (2020) Alternative chloride transport pathways as pharmacological targets for the treatment of cystic fibrosis. J. Cyst. Fibros 19, S37–S41 10.1016/j.jcf.2019.10.020 [PubMed: 31662238]
19. Kere J (2006) Overview of the SLC26 family and associated diseases. Novartis Found. Symp 273, 2–11 PMID:17120758 [PubMed: 17120758]
20. Alper SL and Sharma AK (2013) The SLC26 gene family of anion transporters and channels. Mol. Aspects Med 34, 494–515 10.1016/j.mam.2012.07.009 [PubMed: 23506885]
21. Liu X, Li T and Tuo B (2018) Physiological and pathophysiological relevance of the anion transporter Slc26a9 in multiple organs. Front. Physiol 9, 1197 10.3389/fphys.2018.01197 [PubMed: 30233393]
22. Sharma AK, Rigby AC and Alper SL (2011) STAS domain structure and function. Cell. Physiol. Biochem 28, 407–422 10.1159/000335104 [PubMed: 22116355]
23. Geertsma ER, Chang YN, Shaik FR, Neldner Y, Pardon E, Steyaert J et al. (2015) Structure of a prokaryotic fumarate transporter reveals the architecture of the SLC26 family. Nat. Struct. Mol. Biol 22, 803–808 10.1038/nsmb.3091 [PubMed: 26367249]
24. Gorbunov D, Sturlese M, Nies F, Kluge M, Bellanda M, Battistutta R et al. (2014) Molecular architecture and the structural basis for anion interaction in prestin and SLC26 transporters. Nat. Commun 5, 3622 10.1038/ncomms4622 [PubMed: 24710176]
25. Rapp C, Bai X and Reithmeier RAF (2017) Molecular analysis of human solute carrier SLC26 anion transporter disease-causing mutations using 3-dimensional homology modeling. Biochim. Biophys. Acta Biomembr 1859, 2420–2434 10.1016/j.bbamem.2017.09.016 [PubMed: 28941661]
26. Walter JD, Sawicka M and Dutzler R (2019) Cryo-EM structures and functional characterization of murine Slc26a9 reveal mechanism of uncoupled chloride transport. eLife 8, e46986 10.7554/eLife.46986 [PubMed: 31339488]
27. Lohi H, Lamprecht G, Markovich D, Heil A, Kujala M, Seidler U et al. (2003) Isoforms of SLC26A6 mediate anion transport and have functional PDZ interaction domains. Am. J. Physiol. Cell Physiol 284, C769–C779 10.1152/ajpcell.00270.2002 [PubMed: 12444019]
28. Rossmann H, Jacob P, Baisch S, Hassoun R, Meier J, Natour D et al. (2005) The CFTR associated protein CAP70 interacts with the apical Cl-/HCO3- exchanger DRA in rabbit small intestinal mucosa. Biochemistry 44, 4477–4487 10.1021/bi048828b [PubMed: 15766278]

29. Ohana E, Yang D, Shcheynikov N and Muallem S (2009) Diverse transport modes by the solute carrier 26 family of anion transporters. J. Physiol 587, 2179–2185 10.1113/jphysiol.2008.164863 [PubMed: 19015189]
30. Ko SB, Zeng W, Dorwart MR, Luo X, Kim KH, Millen L et al. (2004) Gating of CFTR by the STAS domain of SLC26 transporters. Nat. Cell Biol 6, 343–350 10.1038/ncb1115 [PubMed: 15048129]
31. Chang MH, Plata C, Sindic A, Ranatunga WK, Chen AP, Zandi-Nejad K et al. (2009) Slc26a9 is inhibited by the R-region of the cystic fibrosis transmembrane conductance regulator via the STAS domain. J. Biol. Chem 284, 28306–28318 10.1074/jbc.M109.001669 [PubMed: 19643730]
32. Bertrand CA, Zhang R, Pilewski JM and Frizzell RA (2009) SLC26A9 is a constitutively active, CFTR-regulated anion conductance in human bronchial epithelia. J. Gen. Physiol 133, 421–438 10.1085/jgp.200810097 [PubMed: 19289574]
33. Avella M, Loriol C, Boulukos K, Borgese F and Ehrenfeld J (2011) SLC26A9 stimulates CFTR expression and function in human bronchial cell lines. J. Cell Physiol 226, 212–223 10.1002/jcp.22328 [PubMed: 20658517]
34. Khouri E E and Toure A (2014) Functional interaction of the cystic fibrosis transmembrane conductance regulator with members of the SLC26 family of anion transporters (SLC26A8 and SLC26A9): physiological and pathophysiological relevance. Int. J. Biochem. Cell Biol 52, 58–67 10.1016/j.biocel.2014.02.001 [PubMed: 24530837]
35. Bertrand CA, Mitra S, Mishra SK, Wang X, Zhao Y, Pilewski JM et al. (2017) The CFTR trafficking mutation F508del inhibits the constitutive activity of SLC26A9. Am. J. Physiol. Lung Cell. Mol. Physiol 312, L912–LL25 10.1152/ajplung.00178.2016 [PubMed: 28360110]
36. Balazs A and Mall MA (2018) Role of the SLC26A9 chloride channel as disease modifier and potential therapeutic target in cystic fibrosis. Front. Pharmacol 9, 1112 10.3389/fphar.2018.01112 [PubMed: 30327603]
37. Corvol H, Mesinele J, Douksieh IH, Strug LJ, Boelle PY and Guillot L (2018) SLC26A9 gene is associated With lung function response to ivacaftor in patients with cystic fibrosis. Front. Pharmacol 9, 828 10.3389/fphar.2018.00828 [PubMed: 30140228]
38. Sato Y, Thomas DY and Hanrahan JW (2019) The anion transporter SLC26A9 localizes to tight junctions and is degraded by the proteasome when co-expressed with F508del-CFTR. J. Biol. Chem 294, 18269–18284 10.1074/jbc.RA119.010192 [PubMed: 31645438]
39. Xu J, Henriksnas J, Barone S, Witte D, Shull GE, Forte JG et al. (2005) SLC26A9 is expressed in gastric surface epithelial cells, mediates Cl-/HCO3- exchange, and is inhibited by NH4+. Am. J. Physiol. Cell Physiol 289, C493–C505 10.1152/ajpcell.00030.2005 [PubMed: 15800055]
40. Dorwart MR, Shcheynikov N, Wang Y, Stippec S and Muallem S (2007) SLC26A9 is a Cl(−) channel regulated by the WNK kinases. J. Physiol 584, 333–345 10.1113/jphysiol.2007.135855 [PubMed: 17673510]
41. Loriol C, Dulong S, Avella M, Gabillat N, Boulukos K, Borgese F et al. (2008) Characterization of SLC26A9, facilitation of Cl(−) transport by bicarbonate. Cell. Physiol. Biochem 22, 15–30 10.1159/000149780 [PubMed: 18769029]
42. Chang MH, Plata C, Zandi-Nejad K, Sindic A, Sussman CR, Mercado A et al. (2009) Slc26a9–anion exchanger, channel and Na+ transporter. J. Membr. Biol 228, 125–140 10.1007/s00232-009-9165-5 [PubMed: 19365592]
43. Salomon JJ, Spahn S, Wang X, Fullekrug J, Bertrand CA and Mall MA (2016) Generation and functional characterization of epithelial cells with stable expression of SLC26A9 Cl- channels. Am. J. Physiol. Lung Cell. Mol. Physiol 310, L593–L602 10.1152/ajplung.00321.2015 [PubMed: 26801567]
44. Chi X, Jin X, Chen Y, Lu X, Tu X, Li X et al. (2020) Structural insights into the gating mechanism of human SLC26A9 mediated by its C-terminal sequence. Cell Discov. 6, 55 10.1038/s41421-020-00193-7 [PubMed: 32818062]
45. Sun L, Rommens JM, Corvol H, Li W, Li X, Chiang TA et al. (2012) Multiple apical plasma membrane constituents are associated with susceptibility to meconium ileus in individuals with cystic fibrosis. Nat. Genet 44, 562–569 10.1038/ng.2221 [PubMed: 22466613]

46. Bakouh N, Bienvenu T, Thomas A, Ehrenfeld J, Liote H, Roussel D et al. (2013) Characterization of SLC26A9 in patients with CF-like lung disease. Hum. Mutat 34, 1404–1414 10.1002/humu.22382 [PubMed: 24272871]
47. Blackman SM, Commander CW, Watson C, Arcara KM, Strug LJ, Stonebraker JR et al. (2013) Genetic modifiers of cystic fibrosis-related diabetes. Diabetes 62, 3627–3635 10.2337/db13-0510 [PubMed: 23670970]
48. Miller MR, Soave D, Li W, Gong J, Pace RG, Boelle PY et al. (2015) Variants in solute carrier SLC26A9 modify prenatal exocrine pancreatic damage in cystic fibrosis. J. Pediatr 166, 1152–1157 e6 10.1016/j.jpeds.2015.01.044 [PubMed: 25771386]
49. Strug LJ, Gonska T, He G, Keenan K, Ip W, Boelle PY et al. (2016) Cystic fibrosis gene modifier SLC26A9 modulates airway response to CFTR-directed therapeutics. Hum. Mol. Genet 25, 4590–4600 10.1093/hmg/ddw290 [PubMed: 28171547]
50. Eastman AC, Pace RG, Dang H, Aksit MA, Vecchio-Pagan B, Lam AN et al. (2021) SLC26A9 SNP rs7512462 is not associated with lung disease severity or lung function response to ivacaftor in cystic fibrosis patients with G551D-CFTR. J. Cyst. Fibros 20, 851–856 10.1016/j.jcf.2021.02.007 [PubMed: 33674211]
51. Anagnostopoulou P, Riederer B, Duerr J, Michel S, Binia A, Agrawal R et al. (2012) SLC26A9-mediated chloride secretion prevents mucus obstruction in airway inflammation. J. Clin. Invest 122, 3629–3634 10.1172/JCI60429 [PubMed: 22945630]
52. Crites KS, Morin G, Orlando V, Patey N, Cantin C, Martel J et al. (2015) CFTR knockdown induces proinflammatory changes in intestinal epithelial cells. J. Inflamm 12, 62 10.1186/s12950-015-0107-y
53. Frayman KB, Armstrong DS, Grimwood K and Ranganathan SC (2017) The airway microbiota in early cystic fibrosis lung disease. Pediatr. Pulmonol 52, 1384–1404 10.1002/ppul.23782 [PubMed: 28815937]
54. Schwiebert EM, Benos DJ, Egan ME, Stutts MJ and Guggino WB (1999) CFTR is a conductance regulator as well as a chloride channel. Physiol. Rev 79, S145–S166 10.1152/physrev.1999.79.1.S145 [PubMed: 9922379]
55. Lohi H, Makela S, Pulkkinen K, Hoglund P, Karjalainen-Lindsberg ML, Puolakkainen P et al. (2002) Upregulation of CFTR expression but not SLC26A3 and SLC9A3 in ulcerative colitis. Am. J. Physiol. Gastrointest. Liver Physiol 283, G567–G575 10.1152/ajpgi.00356.2001 [PubMed: 12181169]
56. Romero MF, Chang MH, Plata C, Zandi-Nejad K, Mercado A, Broumand V et al. (2006) Physiology of electrogenic SLC26 paralogues. Novartis Found. Symp 273, 126–138 PMID:17120765 [PubMed: 17120765]
57. Ousingsawat J, Schreiber R and Kunzelmann K (2012) Differential contribution of SLC26A9 to Cl(−) conductance in polarized and non-polarized epithelial cells. J. Cell Physiol 227, 2323–2329 10.1002/jcp.22967 [PubMed: 21809345]
58. Labbadia J and Morimoto RI (2015) The biology of proteostasis in aging and disease. Annu. Rev. Biochem 84, 435–464 10.1146/annurev-biochem-060614-033955 [PubMed: 25784053]
59. Li X, Shao H, Taylor IR and Gestwicki JE (2016) Targeting allosteric control mechanisms in heat shock protein 70 (Hsp70). Curr. Top. Med. Chem 16, 2729–2740 10.2174/1568026616666160413140911 [PubMed: 27072701]
60. Baranczak A and Kelly JW (2016) A current pharmacologic agent versus the promise of next generation therapeutics to ameliorate protein misfolding and/or aggregation diseases. Curr. Opin. Chem. Biol 32, 10–21 10.1016/j.cbpa.2016.01.009 [PubMed: 26859714]
61. Zhang Y, Nijbroek G, Sullivan ML, McCracken AA, Watkins SC, Michaelis S et al. (2001) Hsp70 molecular chaperone facilitates endoplasmic reticulum-associated protein degradation of cystic fibrosis transmembrane conductance regulator in yeast. Mol. Biol. Cell 12, 1303–1314 10.1091/mbc.12.5.1303 [PubMed: 11359923]
62. Youker RT, Walsh P, Beilharz T, Lithgow T and Brodsky JL (2004) Distinct roles for the Hsp40 and Hsp90 molecular chaperones during cystic fibrosis transmembrane conductance regulator degradation in yeast. Mol. Biol. Cell 15, 4787–4797 10.1091/mbc.e04-07-0584 [PubMed: 15342786]

63. Ahner A, Nakatsukasa K, Zhang H, Frizzell RA and Brodsky JL (2007) Small heat-shock proteins select deltaF508-CFTR for endoplasmic reticulum-associated degradation. Mol. Biol. Cell 18, 806–814 10.1091/mbc.e06-05-0458 [PubMed: 17182856]
64. Needham PG, Mikoluk K, Dhakarwal P, Khadem S, Snyder AC, Subramanya AR et al. (2011) The thiazide-sensitive naCl cotransporter is targeted for chaperone-dependent endoplasmic reticulum-associated degradation. J. Biol. Chem 286, 43611–43621 10.1074/jbc.M111.288928 [PubMed: 22027832]
65. Buck TM, Plavchak L, Roy A, Donnelly BF, Kashlan OB, Kleyman TR et al. (2013) The Lhs1/GRP170 chaperones facilitate the endoplasmic reticulum-associated degradation of the epithelial sodium channel. J. Biol. Chem 288, 18366–18380 10.1074/jbc.M113.469882 [PubMed: 23645669]
66. Kolb AR, Needham PG, Rothenberg C, Guerriero CJ, Welling PA and Brodsky JL (2014) ESCRT regulates surface expression of the Kir2.1 potassium channel. Mol. Biol. Cell 25, 276–289 10.1091/mbc.e13-07-0394 [PubMed: 24227888]
67. O'Donnell BM, Mackie TD, Subramanya AR and Brodsky JL (2017) Endoplasmic reticulum-associated degradation of the renal potassium channel, ROMK, leads to type II Bartter syndrome. J. Biol. Chem 292, 12813–12827 10.1074/jbc.M117.786376 [PubMed: 28630040]
68. Mackie TD, Kim BY, Subramanya AR, Bain DJ, O'Donnell AF, Welling PA et al. (2018) The endosomal trafficking factors CORVET and ESCRT suppress plasma membrane residence of the renal outer medullary potassium channel (ROMK). J. Biol. Chem 293, 3201–3217 10.1074/jbc.M117.819086 [PubMed: 29311259]
69. Mumberg D, Muller R and Funk M (1995) Yeast vectors for the controlled expression of heterologous proteins in different genetic backgrounds. Gene 156, 119–122 10.1016/0378-1119(95)00037-7 [PubMed: 7737504]
70. Brachmann CB, Davies A, Cost GJ, Caputo E, Li J, Hieter P et al. (1998) Designer deletion strains derived from *saccharomyces cerevisiae* S288C: a useful set of strains and plasmids for PCR-mediated gene disruption and other applications. Yeast 14, 115–132 10.1002/(SICI)1097-0061(19980130)14:2<115::AID-YEA204>3.0.CO;2-2 [PubMed: 9483801]
71. Adams A GD, Kaiser CA and Stearns T (1997) Methods in Yeast Genetics: A Cold Spring Harbor Laboratory Course Manual, Cold Spring Harbor Laboratory Press
72. Zhang Y, Michaelis S and Brodsky JL (2002) CFTR expression and ER-associated degradation in yeast. Methods Mol. Med 70, 257–265 10.1385/1-59259-187-6:257 [PubMed: 11917528]
73. Sun Z, Guerriero CJ and Brodsky JL (2021) Substrate ubiquitination retains misfolded membrane proteins in the endoplasmic reticulum for degradation. Cell Rep. 36, 109717 10.1016/j.celrep.2021.109717 [PubMed: 34551305]
74. Hochstrasser M, Ellison MJ, Chau V and Varshavsky A (1991) The short-lived MAT alpha 2 transcriptional regulator is ubiquitinated *in vivo*. Proc. Natl Acad. Sc. U.S.A 88, 4606–4610 10.1073/pnas.88.11.4606 [PubMed: 1647011]
75. Guerriero CJ, Weiberth KF and Brodsky JL (2013) Hsp70 targets a cytoplasmic quality control substrate to the San1p ubiquitin ligase. J. Biol. Chem 288, 18506–18520 10.1074/jbc.M113.475905 [PubMed: 23653356]
76. Wang X, Larsen MB, Frizell RA and Bertrand CA (2016) A Predicted Phosphorylation Site In SLC26A9 Modulates CFTR-Dependent Acitivy Pediatric Pulmonology, Wiley, p. 223
77. Needham PG, Guerriero CJ and Brodsky JL (2019) Chaperoning endoplasmic reticulum-associated degradation (ERAD) and protein conformational diseases. Cold Spring Harb. Perspect. Biol 11, a033928 10.1101/cshperspect.a033928 [PubMed: 30670468]
78. Lohi H, Kujala M, Makela S, Lehtonen E, Kestila M, Saarialho-Kere U et al. (2002) Functional characterization of three novel tissue-specific anion exchangers SLC26A7, -A8, and -A9. J. Biol. Chem 277, 14246–14254 10.1074/jbc.M111802200 [PubMed: 11834742]
79. Sun Z and Brodsky JL (2019) Protein quality control in the secretory pathway. J. Cell Biol 218, 3171–3187 10.1083/jcb.201906047 [PubMed: 31537714]
80. Hirsch C, Gauss R, Horn SC, Neuber O and Sommer T (2009) The ubiquitylation machinery of the endoplasmic reticulum. Nature 458, 453–460 10.1038/nature07962 [PubMed: 19325625]

81. Christianson JC and Ye Y (2014) Cleaning up in the endoplasmic reticulum: ubiquitin in charge. Nat. Struct. Mol. Biol 21, 325–335 10.1038/nsmb.2793 [PubMed: 24699081]
82. Preston GM and Brodsky JL (2017) The evolving role of ubiquitin modification in endoplasmic reticulum-associated degradation. Biochem. J 474, 445–469 10.1042/BCJ20160582 [PubMed: 28159894]
83. Lee DH and Goldberg AL (1996) Selective inhibitors of the proteasome-dependent and vacuolar pathways of protein degradation in *saccharomyces cerevisiae*. J. Biol. Chem 271, 27280–4 10.1074/jbc.271.44.27280 [PubMed: 8910302]
84. Wilhovsky S, Gardner R and Hampton R (2000) HRD gene dependence of endoplasmic reticulum-associated degradation. Mol. Biol. Cell 11, 1697–1708 10.1091/mbc.11.5.1697 [PubMed: 10793145]
85. Swanson R, Locher M and Hochstrasser M (2001) A conserved ubiquitin ligase of the nuclear envelope/endoplasmic reticulum that functions in both ER-associated and Matalpha2 repressor degradation. Genes Dev. 15, 2660–2674 10.1101/gad.933301 [PubMed: 11641273]
86. Raasi S and Wolf DH (2007) Ubiquitin receptors and ERAD: a network of pathways to the proteasome. Semin. Cell Dev. Biol 18, 780–791 10.1016/j.semcdb.2007.09.008 [PubMed: 17942349]
87. Wu X and Rapoport TA (2018) Mechanistic insights into ER-associated protein degradation. Curr. Opin. Cell Biol 53, 22–28 10.1016/j.ceb.2018.04.004 [PubMed: 29719269]
88. Jones EW (1984) The synthesis and function of proteases in *Saccharomyces*: genetic approaches. Annu. Rev. Genet 18, 233–270 10.1146/annurev.ge.18.120184.001313 [PubMed: 6397123]
89. Sun Z and Brodsky JL (2018) The degradation pathway of a model misfolded protein is determined by aggregation propensity. Mol. Biol. Cell 29, 1422–1434 10.1091/mbc.E18-02-0117 [PubMed: 29688814]
90. Nakatsukasa K, Huyer G, Michaelis S and Brodsky JL (2008) Dissecting the ER-associated degradation of a misfolded polytopic membrane protein. Cell 132, 101–112 10.1016/j.cell.2007.11.023 [PubMed: 18191224]
91. Han S, Liu Y and Chang A (2007) Cytoplasmic Hsp70 promotes ubiquitination for endoplasmic reticulum-associated degradation of a misfolded mutant of the yeast plasma membrane ATPase, PMA1. J. Biol. Chem 282, 26140–26149 10.1074/jbc.M701969200 [PubMed: 17631501]
92. Plemper RK, Bohmler S, Bordallo J, Sommer T and Wolf DH (1997) Mutant analysis links the translocon and BiP to retrograde protein transport for ER degradation. Nature 388, 891–895 10.1038/42276 [PubMed: 9278052]
93. Nishikawa SI, Fewell SW, Kato Y, Brodsky JL and Endo T (2001) Molecular chaperones in the yeast endoplasmic reticulum maintain the solubility of proteins for retrotranslocation and degradation. J. Cell Biol 153, 1061–1070 10.1083/jcb.153.5.1061 [PubMed: 11381090]
94. Becker J, Walter W, Yan W and Craig EA (1996) Functional interaction of cytosolic hsp70 and a dnaJ-related protein, Ydj1p, in protein translocation *in vivo*. Mol. Cell. Biol 16, 4378–4386 10.1128/MCB.16.8.4378 [PubMed: 8754838]
95. Kabani M, Kelley SS, Morrow MW, Montgomery DL, Sivendran R, Rose MD et al. (2003) Dependence of endoplasmic reticulum-associated degradation on the peptide binding domain and concentration of BiP. Mol. Biol. Cell 14, 3437–3448 10.1091/mbc.e02-12-0847 [PubMed: 12925775]
96. Heck JW, Cheung SK and Hampton RY (2010) Cytoplasmic protein quality control degradation mediated by parallel actions of the E3 ubiquitin ligases Ubr1 and San1. Proc. Natl Acad. Sci. U.S.A 107, 1106–1111 10.1073/pnas.0910591107 [PubMed: 20080635]
97. Nillegoda NB, Theodoraki MA, Mandal AK, Mayo KJ, Ren HY, Sultana R et al. (2010) Ubr1 and Ubr2 function in a quality control pathway for degradation of unfolded cytosolic proteins. Mol. Biol. Cell 21, 2102–2116 10.1091/mbc.e10-02-0098 [PubMed: 20462952]
98. Hiller MM, Finger A, Schweiger M and Wolf DH (1996) ER degradation of a misfolded luminal protein by the cytosolic ubiquitin-proteasome pathway. Science 273, 1725–1728 10.1126/science.273.5282.1725 [PubMed: 8781238]
99. Zargari A, Boban M, Heessen S, Andreasson C, Thyberg J and Ljungdahl PO (2007) Inner nuclear membrane proteins Asi1, Asi2, and Asi3 function in concert to maintain the latent properties

of transcription factors Stp1 and Stp2. J. Biol. Chem 282, 594–605 10.1074/jbc.M609201200 [PubMed: 17085444]

100. Flagg MP, Wangeline MA, Holland SR, Duttke SH, Benner C, Neal S et al. (2021) Inner-nuclear-membrane-associated degradation employs Dfm1-independent retrotranslocation and alleviates misfolded transmembrane-protein toxicity. Mol. Biol. Cell 32, 521–537 10.1091/mbc.E20-11-0720 [PubMed: 33566711]
101. Dupre S, Urban-Grimal D and Haguenauer-Tsapis R (2004) Ubiquitin and endocytic internalization in yeast and animal cells. Biochim. Biophys. Acta 1695, 89–111 10.1016/j.bbamcr.2004.09.024 [PubMed: 15571811]
102. Urbe S (2005) Ubiquitin and endocytic protein sorting. Essays Biochem. 41, 81–98 10.1042/bse0410081 [PubMed: 16250899]
103. Haynes CM, Caldwell S and Cooper AA (2002) An HRD/DER-independent ER quality control mechanism involves Rsp5p-dependent ubiquitination and ER-Golgi transport. J. Cell Biol 158, 91–101 10.1083/jcb.200201053 [PubMed: 12105183]
104. Wang S, Thibault G and Ng DTW (2011) Routing misfolded proteins through the multivesicular body (MVB) pathway protects against proteotoxicity. J. Biol. Chem 286, 29376–29387 10.1074/jbc.M111.233346 [PubMed: 21708947]
105. Zhao Y, Macgurn JA, Liu M and Emr S (2013) The ART-Rsp5 ubiquitin ligase network comprises a plasma membrane quality control system that protects yeast cells from proteotoxic stress. eLife 2, e00459 10.7554/eLife.00459 [PubMed: 23599894]
106. Fang NN, Chan GT, Zhu M, Comyn SA, Persaud A, Deshaies RJ et al. (2014) Rsp5/Nedd4 is the main ubiquitin ligase that targets cytosolic misfolded proteins following heat stress. Nat. Cell Biol 16, 1227–1237 10.1038/ncb3054 [PubMed: 25344756]
107. Nagy V and Dikic I (2010) Ubiquitin ligase complexes: from substrate selectivity to conjugational specificity. Biol. Chem 391, 163–169 10.1515/bc.2010.021 [PubMed: 20030582]
108. Williamson DS, Borgognoni J, Clay A, Daniels Z, Dokurno P, Drysdale MJ et al. (2009) Novel adenosine-derived inhibitors of 70 kDa heat shock protein, discovered through structure-based design. J. Med. Chem 52, 1510–1513 10.1021/jm801627a [PubMed: 19256508]
109. Kolb AR, Buck TM and Brodsky JL (2011) Saccharomyces cerivisiae as a model system for kidney disease: what can yeast tell us about renal function? Am. J. Physiol. Renal Physiol 301, F1–11 10.1152/ajprenal.00141.2011 [PubMed: 21490136]
110. Varga K, Jurkuvenaite A, Wakefield J, Hong JS, Guimbellot JS, Venglarik CJ et al. (2004) Efficient intracellular processing of the endogenous cystic fibrosis transmembrane conductance regulator in epithelial cell lines. J. Biol. Chem 279, 22578–22584 10.1074/jbc.M401522200 [PubMed: 15066992]
111. Vashist S and Ng DT (2004) Misfolded proteins are sorted by a sequential checkpoint mechanism of ER quality control. J. Cell Biol 165, 41–52 10.1083/jcb.200309132 [PubMed: 15078901]
112. Buck TM, Kolb AR, Boyd CR, Kleyman TR and Brodsky JL (2010) The endoplasmic reticulum-associated degradation of the epithelial sodium channel requires a unique complement of molecular chaperones. Mol. Biol. Cell 21, 1047–1058 10.1091/mbc.e09-11-0944 [PubMed: 20110346]
113. Bernasconi R, Galli C, Calanca V, Nakajima T and Molinari M (2010) Stringent requirement for HRD1, SEL1L, and OS-9/XTP3-B for disposal of ERAD-LS substrates. J. Cell Biol 188, 223–235 10.1083/jcb.200910042 [PubMed: 20100910]
114. Grove DE, Rosser MF, Ren HY, Naren AP and Cyr DM (2009) Mechanisms for rescue of correctable folding defects in CFTRDelta F508. Mol. Biol. Cell 20, 4059–4069 10.1091/mbc.e08-09-0929 [PubMed: 19625452]
115. Chung WJ, Goeckeler-Fried JL, Havasi V, Chiang A, Rowe SM, Plyler ZE et al. (2016) Increasing the endoplasmic reticulum pool of the F508del allele of the cystic fibrosis transmembrane conductance regulator leads to greater folding correction by small molecule therapeutics. PLoS ONE 11, e0163615 10.1371/journal.pone.0163615 [PubMed: 27732613]
116. Huyer G, Piluek WF, Fansler Z, Kreft SG, Hochstrasser M, Brodsky JL et al. (2004) Distinct machinery is required in *saccharomyces cerevisiae* for the endoplasmic reticulum-associated

degradation of a multispanning membrane protein and a soluble luminal protein. J. Biol. Chem 279, 38369–38378 10.1074/jbc.M402468200 [PubMed: 15252059]

117. Sato BK, Schulz D, Do PH and Hampton RY (2009) Misfolded membrane proteins are specifically recognized by the transmembrane domain of the Hrd1p ubiquitin ligase. Mol. Cell 34, 212–222 10.1016/j.molcel.2009.03.010 [PubMed: 19394298]
118. Dohmen RJ, Wu P and Varshavsky A (1994) Heat-inducible degron: a method for constructing temperature-sensitive mutants. Science 263, 1273–1276 10.1126/science.8122109 [PubMed: 8122109]
119. Kelly JW (2020) Pharmacologic approaches for adapting proteostasis in the secretory pathway to ameliorate protein conformational diseases. Cold Spring Harb. Perspect. Biol 12, a034108 10.1101/cshperspect.a034108 [PubMed: 31088828]

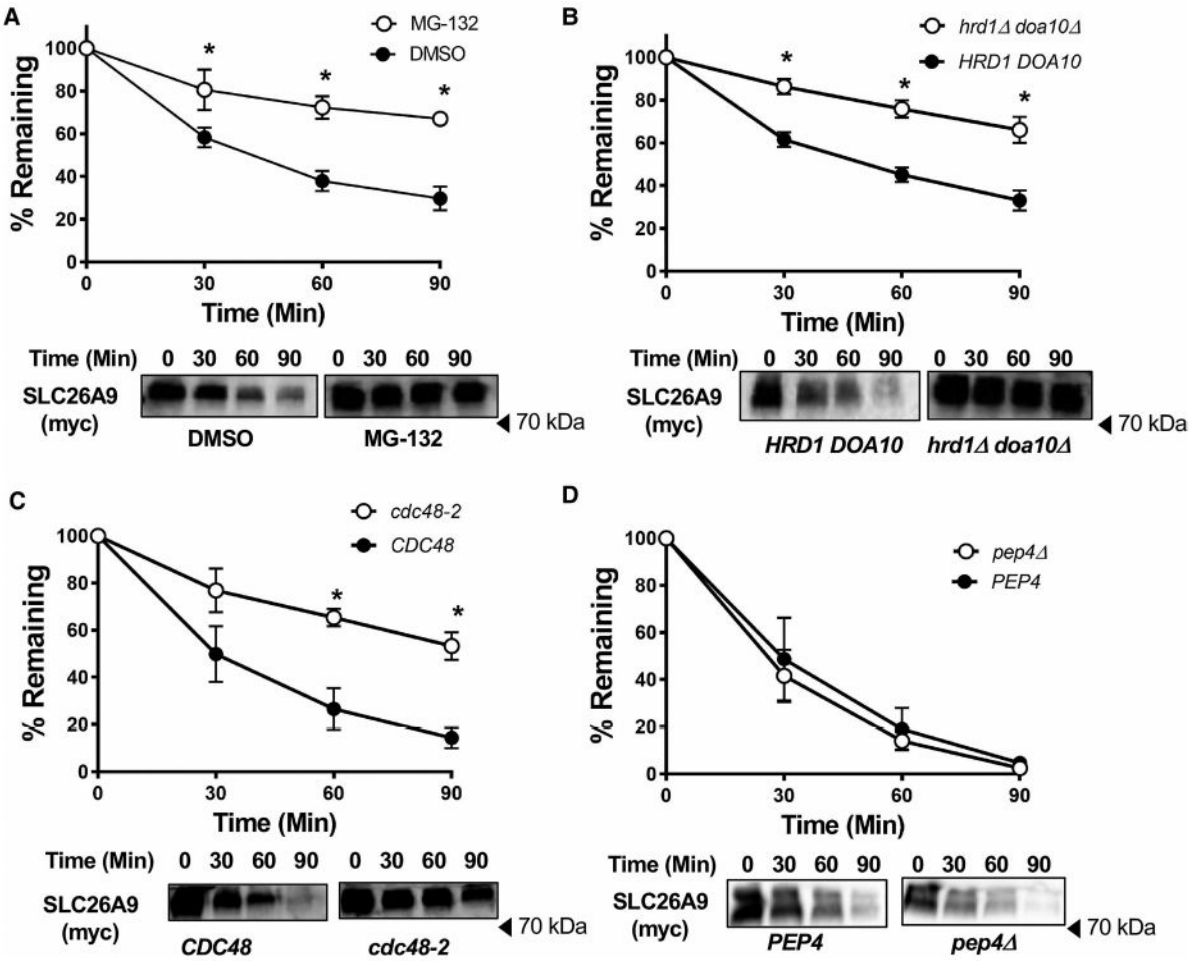

Figure 1. SLC26A9 is an ERAD substrate in yeast.

The stability of SLC26A9 in the indicated wild-type and mutant strains was determined in cycloheximide chase assays. (**A**) SLC26A9 was expressed in a *pdr5Δ* strain, and cells were pre-treated for 30 min with either the vehicle (DMSO) or with 100 μM MG-132, as indicated. (**B**) SLC26A9 degradation was measured in wild-type and *hrd1Δ doa10Δ* yeast. (**C**) SLC26A9 degradation was measured in wild-type and *cdc48-2* yeast after cells were pre-shifted to 38°C for 2 h. (**D**) The vacuolar dependence of SLC26A9 in the wild-type and a *pep4Δ* mutant strain was examined at 30°C. Please note that the background strains used in parts (**A**) and (**D**) were distinct, and thus the relative rates of ERAD differ. In all experiments closed circles represent the wild-type yeast and open circles represent the corresponding mutant yeast strain or cells treated with MG-132, as indicated. A representative immunoblot corresponding to the quantified data is also shown below each graph. The data represent the means ± SEM for 3–6 independent experiments. $*P < 0.05$.

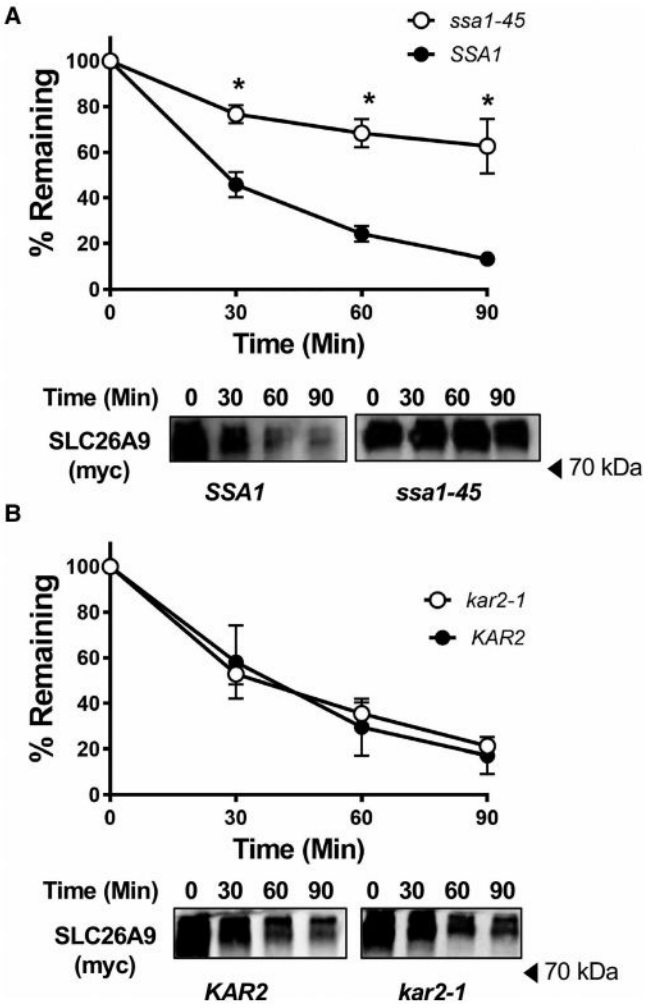

Figure 2. The activity of the cytosolic Hsp70 chaperone is required for SLC26A9 degradation.

The stability of SLC26A9 in the indicated wild-type and mutant strains was determined in cycloheximide chase assays. (**A**) SLC26A9 degradation in *SSA1* yeast and *ssa1–45* (the Hsp70 mutant) strain was measured after cells were pre-shifted to 37°C for 30 min. (**B**) SLC26A9 degradation in wild-type and *kar2-1* (BiP) mutant yeast was measured at 30°C. In all experiments, closed circles represent the wild-type yeast and open circles represent the corresponding mutant yeast strain. A representative immunoblot corresponding to the quantified data is also shown below each graph. The data represent the means ± SEM for 3–6 independent experiments. $*P < 0.05$.

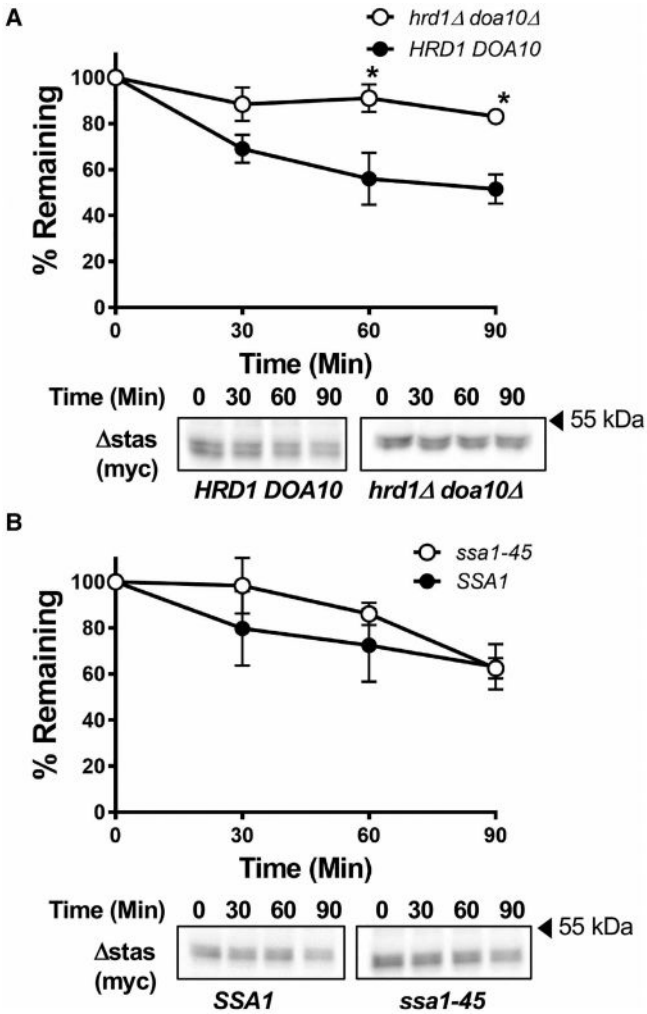

Figure 3. The ERAD of the SLC26A9 transmembrane domain, Δstas, is Hsp70-independent.

The stability of the Δstas construct in the indicated wild-type and mutant strains was determined by cycloheximide chase assay in (**A**) wild-type and *hrd1Δdoa10Δ* mutant yeast at 30°C, and (**B**) *SSA1* and *ssa1–45* strains after cells had been pre-shifted to 37°C for 30 min. In all experiments, closed circles represent the wild-type yeast and open circles represent the corresponding mutant strain. A representative immunoblot corresponding to the quantified data is also shown below each graph. The data represent the means ± SEM for three independent experiments. $*P < 0.05$.

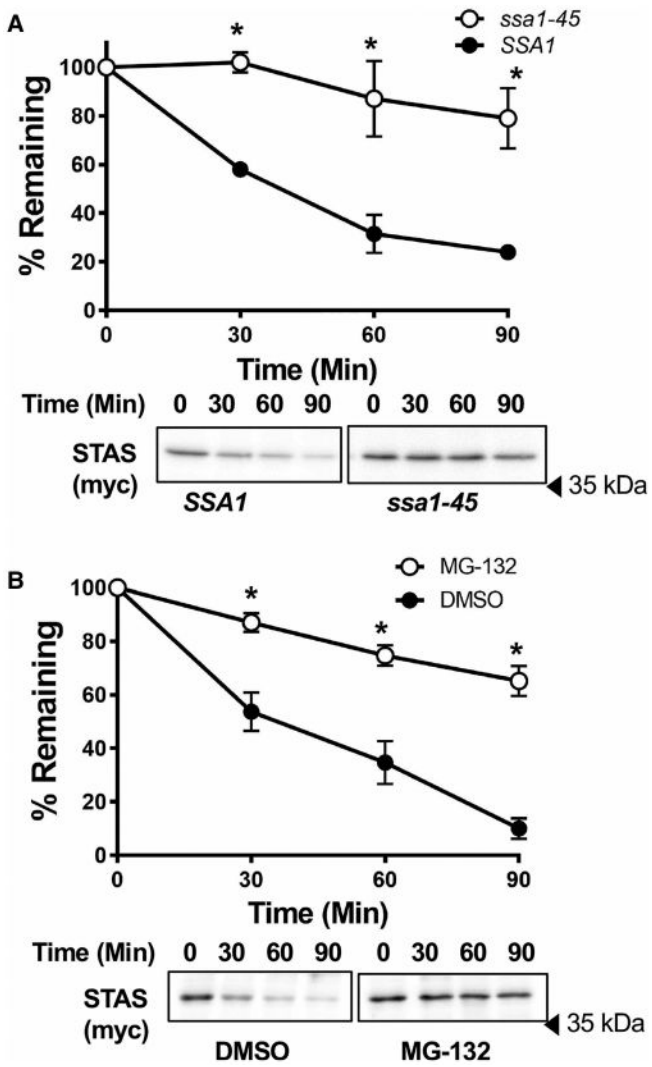

Figure 4. The degradation of the STAS domain is cytosolic Hsp70- and proteasome-dependent.

The stability of the STAS domain in the indicated wild-type and mutant strains was determined by cycloheximide chase assay in (**A**) *SSA1* and *ssa1–45* strains after pre-shift to 37°C for 30 min, and (**B**) *pdr5Δ* cells that were either pre-treated with DMSO or with 100 μM MG-132, as indicated, for 30 min. In all experiments closed circles represent the wild-type yeast (or the DMSO treated cells) and open circles represent the corresponding mutant yeast strain (or MG-132). A representative immunoblot corresponding to the quantified data is also shown below each graph. The data represent the means ± SEM for 3–6 independent experiments. $*P < 0.05$.

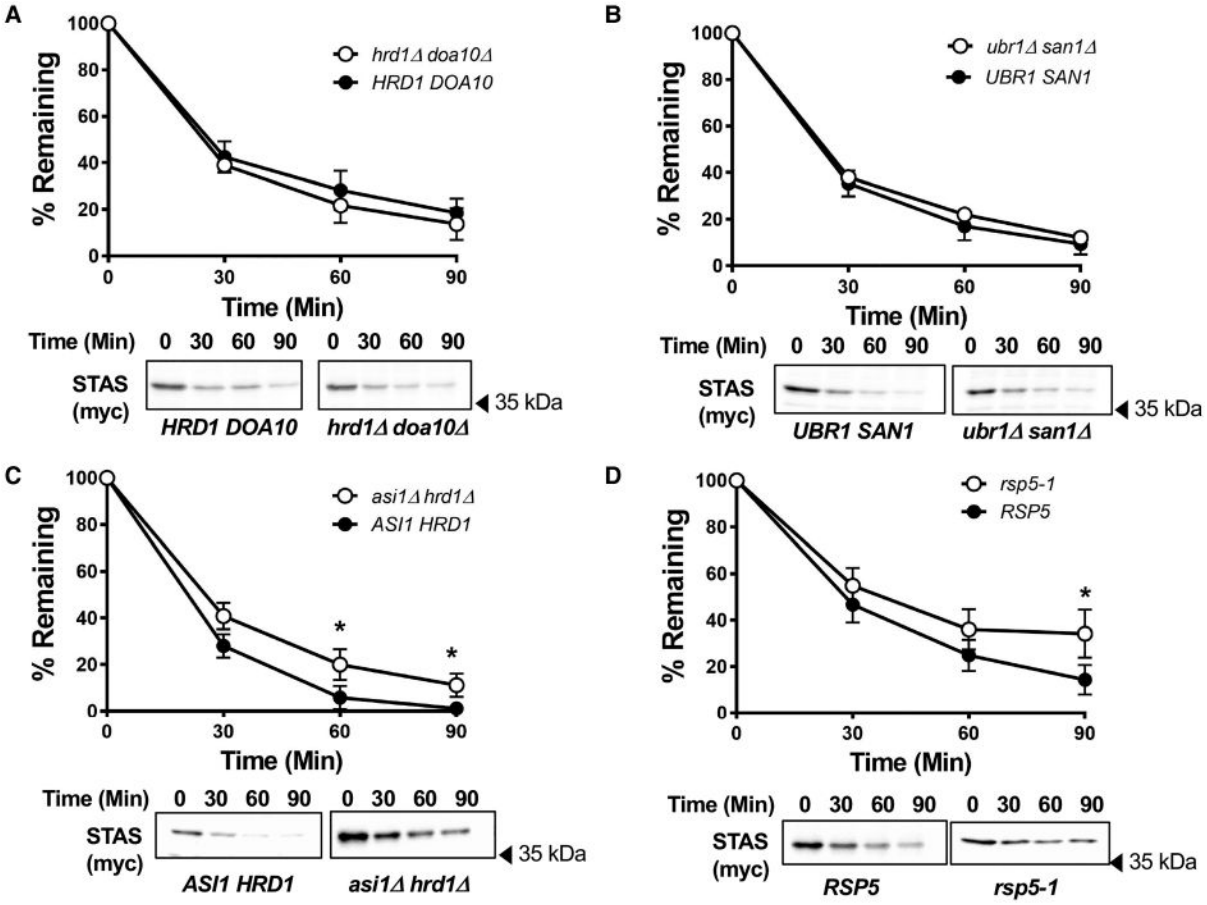

Figure 5. Analysis of the E3 ubiquitin ligase requirements for the degradation of the STAS domain.

The stability of the STAS domain in the indicated wild-type and mutant strains was determined by cycloheximide chase assay in (**A**) wild-type and *hrd1Δ doa10Δ* mutant yeast, (**B**) wild-type and *ubr1Δ san1Δ* mutant yeast, (**C**) wild-type and *asi1Δ hrd1Δ* mutant yeast, and (**D**) wild-type and *rsp5-1* mutant yeast at 38°C after cells were pre-shifted to 38°C for 30 min. In all experiments closed circles represent the wild-type yeast (or the DMSO treated cells) and open circles represent the corresponding mutant yeast strain (or those treated with MG-132). A representative immunoblot corresponding to the quantified data is also shown below each graph. The data represent the means ± SEM for 3–6 independent experiments. *$P < 0.05$.

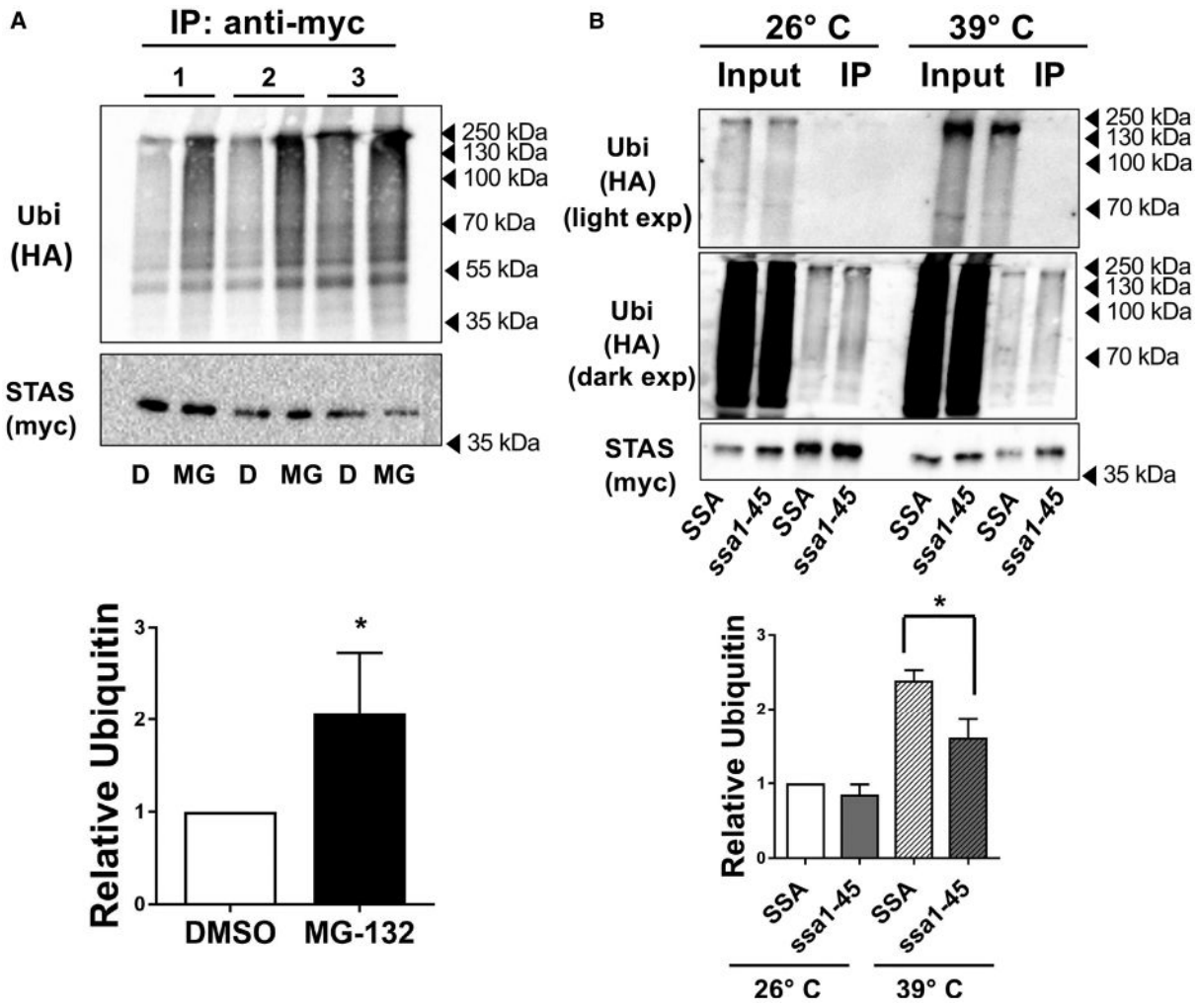

Figure 6. STAS domain ubiquitination is Hsp70-dependent.

The STAS domain was co-expressed with HA epitope-tagged ubiquitin and the domain was immunoprecipitated with anti-myc agarose from whole cell yeast lysates prepared from the indicated strains under denaturing conditions. The ubiquitination of the STAS was determined after immunoprecipitation by blotting for HA-ubiquitin and normalizing the signal to the amount of myc-tagged STAS protein. (**A**) *pdr5Δ* yeast were pre-treated with either DMSO ('D') or with 100 μM MG-132 ('MG') for 1 h prior to cell lysis and the denaturing immunoprecipitation. The graph below the image represents the averaged ubiquitin signal for the data obtained from this experiment performed with three independent cultures (numbered 1, 2, and 3) and for each treatment relative to the amount of STAS protein. Data were normalized to the amount of ubiquitination in the DMSO control. (**B**) Wild-type *SSA1* or *ssa1–45* mutant yeast were grown at 26°C or 39°C for 30 min prior to cell lysis and denaturing immunoprecipitation. The input and immunoprecipitated material (IP) for a representative experiment is shown. Both light and dark exposures of the HA-ubiquitin blot are also shown. The average ubiquitin signal relative to the amount of immunoprecipitated STAS protein was calculated and then normalized to the signal in wild-type yeast at 26°C. The graph below the blots represents the means ± SEM of four

independent experiments for the wild-type (white) and *ssa1–45* mutant (grey) at 26°C, or wild-type (hatched), and *ssa1–45* mutant (grey hatched) after cells had been shifted to 39°C.

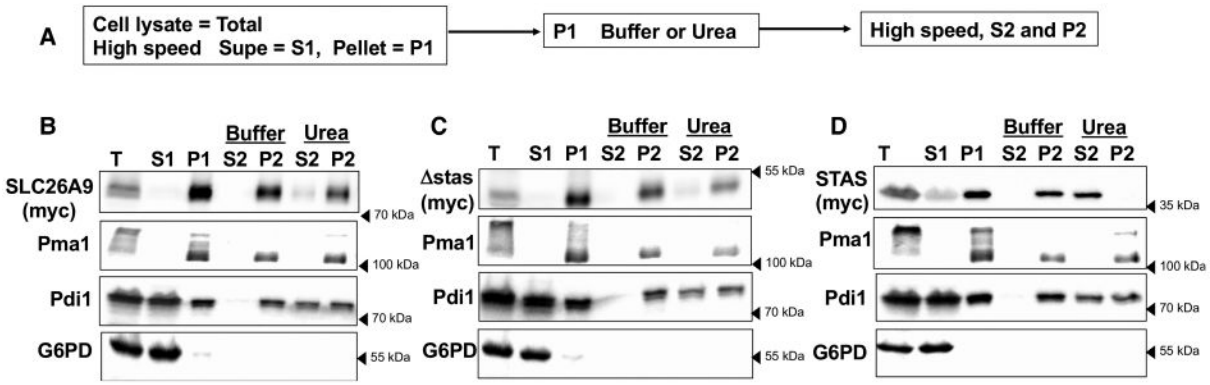

Figure 7. The STAS domain is membrane-associated.

Full length SLC26A9, the transmembrane-rich region of SLC26A9 (Δstas), or the STAS domain were expressed in wild-type yeast and whole cell lysates were prepared and fractionated by centrifugation. (**A**) A flow-chart of the fractionation protocol is shown. Clarified total cell lysate (T) was subjected to a high-speed spin to resolve a supernatant (S1) and pellet (P1) fraction. The (P1) fraction was resuspended in either lysis buffer or lysis buffer containing 6M urea. The treated P1 was then subjected to a second high-speed spin to generate a supernatant (S2) and pellet (P2) fraction. Aliquots of all fractions were then examined by SDS–PAGE and western blotting. Results are shown for the (**B**) SLC26A9 full-length protein, (**C**) the transmembrane-rich region (Δstas), and (**D**) the STAS domain. Controls included Pma1 (an integral membrane protein), Pdi1 (a peripheral membrane protein), and G6PD (a soluble protein), and their behavior in this analysis is shown for each experiment.

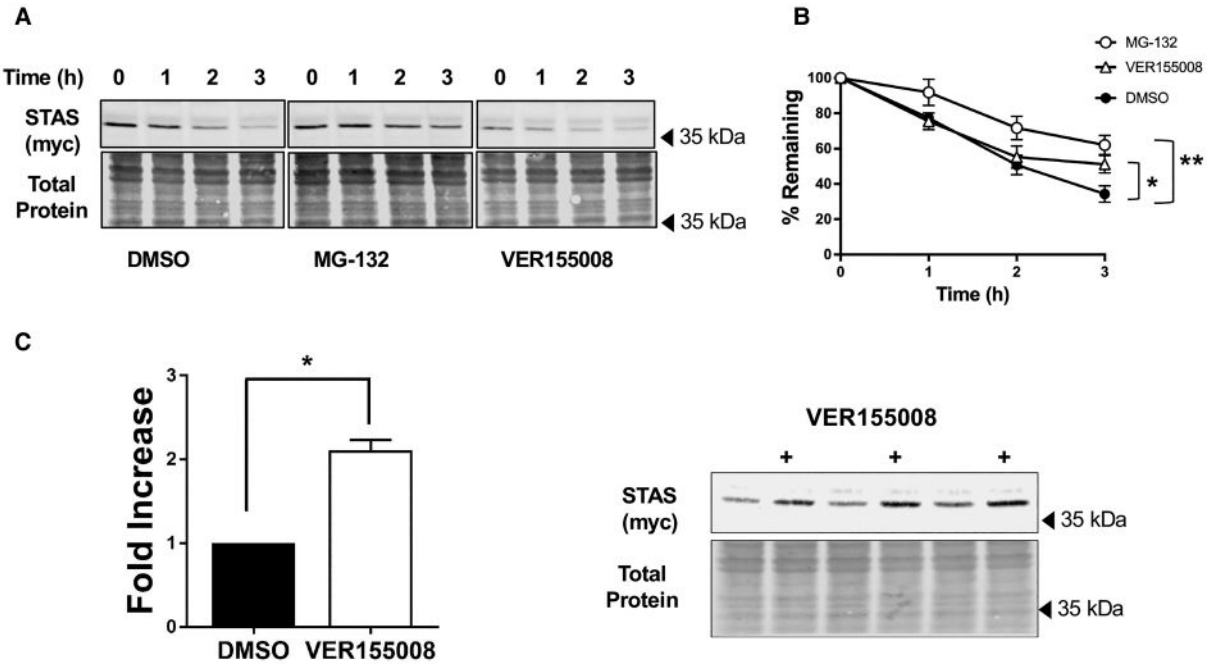

Figure 8. STAS domain degradation in HEK293 cells is also proteasome- and Hsp70- dependent.

The STAS domain was transiently expressed in transfected HEK293 cells and stability was determined in a cycloheximide chase assay. (**A**) HEK293 cells were pre-treated for 2 h with 10 μM MG-132 to build-up the levels of the unstable STAS domain, and the cells were then incubated with DMSO, 10 μM MG-132, or 25 μM of the Hsp70 inhibitor, VER155008. A representative immunoblot corresponding to the quantified data is shown. (**B**) Quantified data based on four independent experiments is shown, ±SEM.*$P < 0.05$, **$P < 0.005$. (**C**) Steady state levels of the STAS protein in HEK293 cells are presented after a 2 h treatment with DMSO or 25 μM VER155008. *Left*, the graph represents the fold increase in STAS after VER155008 treatment compared with the DMSO control. *Right*, the primary data showing the relative levels of the STAS domain as well as the total protein loaded. Note that in this experiment the lag-time observed in parts **A** and **B** was absent, most likely due to uncharacterized antagonistic effects due to MG-132 pre-treatment. This is apparent by the overall decreased levels of the STAS domain in part **A**. Data represent the means ± SEM for three independent experiments. *$P < 0.05$.